Steel and Composite Structures, Vol. 11, No. 6 (2011) 435-454
DOI: http://dx.doi.org/10.12989/scs.2011.11.6.435

Effect of tapered-end shape of FRP sheets on stress concentration in strengthened beams

Khalil Belakhdar[1]*, Abdelouahed Tounsi[2], El Abbes Adda Bedia[2], and Yeghnem Redha[1]

[1]*Departement of Civil Engineering and Hydraulics, University of Saida, BP138 cité Nacer,20000 Saida, Algeria*
[2]*Laboratoire des Matériaux et Hydrologie, Université de Sidi Bel Abbes, BP 89 Cité Ben M'hidi, 22000 Sidi Bel Abbes, Algeria*

(Received November 05, 2010, Revised May 02, 2011, Accepted July 08, 2011)

Abstract. Bonding composite materials to structural members for strengthening purpose has received a considerable attention in recent years. The major problem when using bonded FRP or steel plates to strengthen existing structures is the high interfacial stresses that may be built up near the plate ends which lead to premature failure of the structure. As a result, many researchers have developed several analytical methods to predict the interface performance of bonded repairs. In this paper, a numerical solution using finite - difference method is used to calculate the interfacial stress distribution in beams strengthened with FRP plate having a tapered ends with different thinning profiles. These latter, can significantly reduce the stress concentration. In the present theoretical analysis, the adherend shear deformations are taken into account by assuming a parabolic shear stress through the thickness of both beam and bonded plate. Numerical results from the present analysis are presented to demonstrate the advantages of use the tapers in design of strengthened beams.

Keywords: plate bonding; FRP composite; interfacial stresses; repaired beam; design; taper

1. Introduction

Extensive research and development, over the past decades, in the field of materials engineering and science have been carried out with fibre - reinforced plastic (FRP) composites leading to a wide range of practical applications (Seible *et al*. 1997, Mo *et al*. 1998, Li *et al*. 2006, Wu and Wang 2010) As a nation's infrastructure ages, one of the major challenges the construction industry faces is that the number of deficient structures continues to grow. The applications of using externally bonded FRP plates to reinforced concrete (RC) or steel structures have shown that the technique is effective, efficient and offers a practical solution to this pressing problem. Retrofitting using externally bonded plates is quick, easy with respect to material handling, causes minimal site disruption and produces only little changes in section size. In recent years, many studies have been carried out on the behaviour and strength of such retrofitting method (Roberts 1989, Malek *et al*. 1998, Smith and Teng 2001, Pesic and Pilakoutas 2005, Stratford and Cadei 2006, Hashemi *et al*. 2008, Yuan and Lin 2009, Zhu and Zhang 2010). However, the disadvantage of this technique is that the strengthened members are susceptible to stresses concentration near the plate end, which may cause a total debonding between the member and the FRP plate. Some researchers note that

* Corresponding author, Ph, D., Email: be.khalil@gmail.com

reducing the FRP or steel plate thickness near the plate end is an effective method to minimize the interfacial stresses (Stratford and Cadei 2006, Gao *et al*. 2006).

As a further development of the solutions by Smith (2001), Deng (2004), Stratford (2006), Tounsi (2006), Hashemi *et al*. (2008) and Lee *et al*. (2008), this paper presents a simple numerical solution for obtaining the shear and the normal stresses in the adhesive layer of a retrofitted beam under externally loads. The method can be used to design strengthened beams with section properties that change along the beam such as tapered plates. Finally, a parametric study was conducted to compare the results of models with different geometries.

2. Basic assumptions

The following assumptions were made in the analytical study:

- All materials considered as linear elastic.
- The beam is simply supported and shallow, i.e., plane sections remain plane in bending.
- No slip is allowed at the interface of the bond (i.e., there is a perfect bond at the adhesive steel or FRP plate interface).
- Bending deformations of the adhesive are neglected.
- Stresses in the adhesive layer do not change with the thickness.
- The shear stress analysis assumes that the curvatures in the beam and plate are equal (since this allows the shear stress and peel stress equations to be uncoupled).
- A parabolic shear stress distribution through the depth of both the concrete beam and the bonded plate is assumed.
- In case of reinforced concrete beams, the section properties were based on the uncracked section, excluding the conventional steel reinforcement.

3. Shear stress distribution along the FRP–beam interface

The present stresses derivations are mainly based on Tounsi *et al*. (2009) method. However, the final governing differential equations are solved using finite difference method in order to avoid complex solution in case of tapered plates.

A differential section, dx, can be cut out from the FRP-strengthened beam as shown in Figs. 1 and 2. The strains in the beam near the adhesive interface and the external FRP reinforcement can be expressed, respectively as

$$\varepsilon_1(x) = \frac{du_1(x)}{dx} = \varepsilon_1^M(x) + \varepsilon_1^N(x) \tag{1}$$

$$\varepsilon_2(x) = \frac{du_2(x)}{dx} = \varepsilon_2^M(x) + \varepsilon_2^N(x) \tag{2}$$

Where $u_1(x)$ and $u_2(x)$ are the longitudinal displacements at the base of adherend 1 and the top of adherend 2, respectively. $\varepsilon_1^M(x)$ and $\varepsilon_2^M(x)$ are the strains induced by the bending moment at adherends1and 2, respectively and they are written as follows

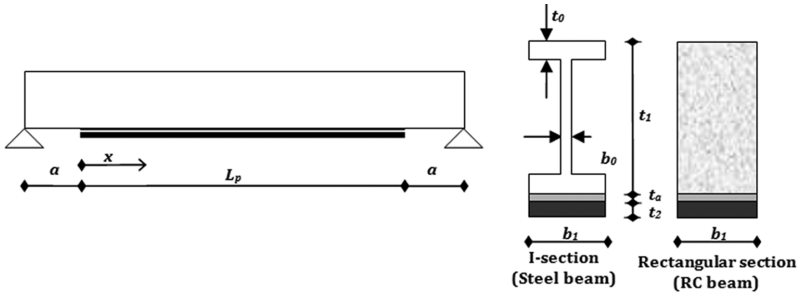

Fig. 1 Simply supported beam strengthened with bonded FRP plate

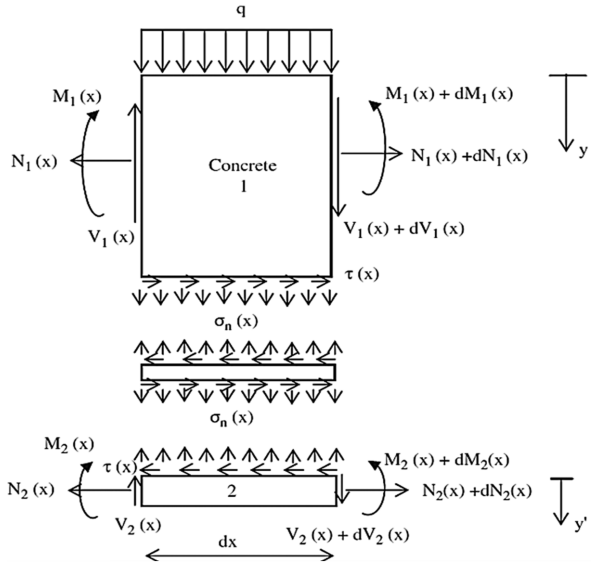

Fig. 2 Forces in infinitesimal element of a soffit - plated beam

$$\varepsilon_1^M(x) = \frac{y_1}{E_1 I_1} M_1(x),\ \varepsilon_2^M(x) = \frac{-y_2}{E_2 I_2} M_2(x) \tag{3}$$

Where E is the elastic modulus and I the second moment of area. The subscripts 1 and 2 denote adherends 1 and 2, respectively. $M(x)$ is the bending moment while y_1 and y_2 are the distances from the bottom of adherend 1 and the top of adherend 2 to their respective centroid. $\varepsilon_1^N(x)$ and $\varepsilon_2^N(x)$ are the unknown longitudinal strains of the beam and FRP reinforcement, respectively, at the adhesive interface and they are due to the longitudinal forces. These strains are given as follows

$$\varepsilon_1^N(x) = \frac{du_1^N(x)}{dx},\ \varepsilon_2^N(x) = \frac{du_2^N(x)}{dx} \tag{4}$$

Where $u_1^N(x)$ and $u_2^N(x)$ represents the longitudinal force-induced adhesive displacement at the interface between the upper (lower) adherend and the adhesive.

To determine the unknown longitudinal strains $\varepsilon_1^N(x)$ and $\varepsilon_2^N(x)$, shear deformations of the adherends

are incorporated in this analysis. It is reasonable to assume that the shear stresses, which develop in the adhesive, are continuous across the adhesive-adherend interface. In addition, equilibrium requires the shear stress to be zero at the free surface. Using the same methodology developed by Tsai *et al*. (1998) and Tounsi (2006), this effect is taken into account. A cubic variation of longitudinal displacements $U_1^N(x,y)$ and $U_2^N(x,y)$ in both adherends is assumed

$$U_1^N(x,y) = A_1(x)y^3 + B_1(x)y + C_1(x) \tag{5}$$

$$U_2^N(x,y') = A_2(x)y'^3 + B_2(x)y' + C_2(x) \tag{6}$$

Where $y(y')$ is a local coordinate system with the origin at the top surface of the upper (lower) adherend (Fig. 2).
The shear stresses in the two adherends are given by

$$\sigma_{xy(1)} = G_1\gamma_{xy(1)} \tag{7}$$

$$\sigma_{xy'(2)} = G_1\gamma_{xy'(2)} \tag{8}$$

$$\gamma_{xy(i)} = \frac{\partial U_i^N}{\partial y} + \frac{\partial w_i^N}{\partial y}, i = 1,2 \tag{9}$$

G_1 and G_2 are the transverse shear moduli of adherends 1 and 2, respectively. Neglecting the variations of transverse displacement W_i^N (induced by the longitudinal forces) with the longitudinal coordinate

$$\gamma_{xy(i)} \approx \frac{\partial U_i^N}{\partial y} \tag{10}$$

The shear stresses are given by

$$\sigma_{xy(1)} = G_1(3A_1(x)y^2 + B_1(x)) \tag{11}$$

$$\sigma_{xy'(2)} = G_2(3A_2(x)y'^2 + B_2(x)) \tag{12}$$

The shear stresses must satisfy the following conditions

$$\sigma_{xy(1)}(x,t_1) = \sigma_{xy'(2)}(x,0) = \tau(x) = \tau_a \tag{13}$$

$$\sigma_{xy(1)}(x,0) = 0, \sigma_{xy'(2)}(x,t_2) = 0 \tag{14}$$

where t_1 and t_2 are the thickness of adherends 1 and 2, respectively.

Condition (13) follows from continuity and assumption of uniform shear stresses ($\tau(x) = \tau_a$) through the thickness of adhesive. Condition (Eq. (14)) states there is no shear stress at the top surface of the adherend 1 (i.e., at $y = 0$) and the bottom surface of adherend 2 (i.e., at $y' = 0$). These conditions yield

$$\sigma_{xy(1)} = \frac{\tau_a}{t_1^2} y^2 \tag{15}$$

$$\sigma_{xy'(1)} = \left(1 - \frac{y'^2}{t_2^2}\right) \tau_a \tag{16}$$

Then, with a linear material constitutive relationship, the adherend shear strain γ_1 for adherend 1 and γ_2 for adherend 2 are written as

$$\gamma_{xy(1)} = \gamma_1 = \frac{\tau_a}{G_1 t_1^2} y^2 \tag{17}$$

$$\gamma_{xy'(2)} = \gamma_2 = \frac{\tau_a}{G_2}\left(1 - \frac{y'^2}{t_2^2}\right) \tag{18}$$

The longitudinal displacement functions U_1^N for the upper adherend and U_2^N for the lower adherend, due to the longitudinal forces, are given as

$$U_1^N(y) = U_1^N(0) + \int_0^y \gamma_1(y)dy = U_1^N(0) + \frac{\tau_a}{3G_1 t_1^2} y^3 \tag{19}$$

$$U_2^N(y') = u_2^N + \int_0^{y'} \gamma_2(y')dy' = u_2^N + \frac{\tau_a}{G_2}\left(y' - \frac{y'^3}{3t_2^2}\right) \tag{20}$$

where $U_1^N(0)$ represents the displacement at the top surface of the upper adherend (due to the longitudinal forces) and u_2^N is the longitudinal force-induced adhesive displacement at the interface between the adhesive and lower adherend.

Note that due to the perfect bonding of the joints, the displacements are continuous at the interfaces between the adhesive and adherends. As a result, u_2^N should be equivalent to the lower adherend displacement at the interface and (the adhesive displacement at the interface between the adhesive and upper adherend) should be the same as the upper adherend displacement at the interface. Based on Eq. (19), u_1^N can be expressed as

$$u_1^N = U_1^N(y = t_1) = U_1^N(0) + \frac{\tau_a t_1}{3G_1} \tag{21}$$

Using Eq. (21), Eq. (19) can be rewritten as

$$U_1^N(y) = u_1^N + \frac{\tau_a}{3G_1 t_1^2} y^3 - \frac{\tau_a t_1}{3G_1} \tag{22}$$

The longitudinal resultant forces, N_1 and N_2, for the upper and lower adherends, respectively, are

$$N_1 = b_1 \int_0^{t_0} \sigma_1^N(y)dy + b_0 \int_{t_0}^{t_1-t_0} \sigma_1^N(y)dy + b_1 \int_{t_1-t_0}^{t_1} \sigma_1^N(y)dy \tag{23}$$

$$N_2 = b_2 \int_0^{t_2} \sigma_2^N(y')dy' \tag{24}$$

Where σ_1^N and σ_2^N are longitudinal normal stresses for the upper and lower adherends, respectively. By changing these stresses into functions of displacements and substituting Eqs. (20) and (22) into the displacements, Eqs. (23) and (24) can be rewritten as

$$\begin{aligned} N_1 &= E_1 b_1 \int_0^{t_1} \frac{dU_1^N}{dx}dy + E_1 b_0 \int_{t_0}^{t_1-t_0} \frac{dU_1^N}{dx}dy + E_1 b_1 \int_{t_1-t_0}^{t_1} \frac{dU_1^N}{dx}dy \\ &= E_1 A_1 \frac{dU_1^N(x)}{dx} - \frac{E_1}{t_1 G_1}\left(\frac{1}{3}t_0(2-t_0)\left(\frac{1}{2}t_1 + t_0\right)(b_1 - b_0) + \frac{1}{4}b_0 t_1^3\right)\frac{d\tau_0(x)}{dx} \end{aligned} \tag{25}$$

$$\text{And, } N_2 = E_2 b_2 \int_0^{t_2} \frac{dU_2^N}{dx}dy' = E_2 A_2\left(\frac{dU_2^N}{dx} + \frac{5t_2}{12G_2}\frac{d\tau a}{dx}\right) \tag{26}$$

Hence, the longitudinal strains induced by the longitudinal forces (Eq. (4)) can be written as

$$\varepsilon_1^N(x) = \frac{dU_1^N(x)}{dx} = \frac{N_1}{E_1 A_1} + \frac{1}{t_1 G_1 A_1}\left(\frac{1}{3}t_0(2t_1 - t_0)\left(\frac{1}{2}t_1 + t_0\right)(b_1 - b_0) + \frac{1}{4}b_0 t_1^3\right)\frac{d\tau a}{dx} \tag{27}$$

$$\varepsilon_2^N(x) = \frac{dU_2^N(x)}{dx} = \frac{N_2}{E_2 A_2} - \frac{5t_2}{12G_2}\frac{d\tau a}{dx} \tag{28}$$

Substituting Eqs. (27), (28) and (3) into Eqs. (1) and (2), respectively, Eq. (4) can be expressed as

$$\varepsilon_1(x) = \frac{dU_1(x)}{dx} = \frac{y_1}{E_1 I_1}M_1(x) + \frac{N_1(x)}{E_1 A_1} + \frac{1}{t_1 G_1 A_1}\left(\frac{1}{3}t_0(2t_1 - t_0)\left(\frac{1}{2}t_1 + t_0\right)(b_1 - b_0) + \frac{1}{4}b_0 t_1^3\right)\frac{d\tau(x)}{dx} \tag{29}$$

$$\varepsilon_2(x) = \frac{du_2(x)}{dx} = \frac{-y_2}{E_2 I_2}M_2(x) + \frac{N_2(x)}{E_2 A_2} - \frac{5t_2}{12G_2}\frac{d\tau(x)}{dx} \tag{30}$$

Where *N(x)* is the axial force in each adherend and *A* is the cross-sectional area.
The shear stress in the adhesive can be expressed as follows

$$\tau_a = \tau(x) = K_S[u_2(x) - u_1(x)] \tag{31}$$

Where $K_S = G_a / t_a$ is shear stiffness of the adhesive, G_a and t_a are shear modulus and thickness of the adhesive, respectively, and $u_1(x)$ and $u_2(x)$ are the longitudinal displacements at the base of adherend 1 and the top of adherend 2. Differentiating the above expression we obtain

$$\frac{d\tau(x)}{dx} = K_S\left[\frac{du_2(x)}{dx} - \frac{du_1(x)}{dx}\right] \tag{32}$$

Consideration of horizontal equilibrium gives

$$\frac{dN_1(x)}{dx} = -b_2\,\tau(x) \tag{33}$$

$$\frac{dN_2(x)}{dx} = b_2\,\tau(x) \tag{34}$$

Where

$$N_2(x) = N(x) = b_2\int_0^x \tau(x) \tag{35}$$

$$N_1(x) = -N(x) = -b_2\int_0^x \tau(x) \tag{36}$$

and b_2 is the width of the FRP plate.

Assuming equal curvature in the beam and the FRP plate, the relationship between the moments in the two adherends can be expressed as

$$M_1(x) = RM_2(x) \tag{37}$$

$$\text{With, } R = \frac{E_1 I_1}{E_2 I_2} \tag{38}$$

Moment equilibrium of the differential segment of the plated beam in Fig. 3 gives

$$M_T(x) = M_1(x) + M_2(x) + N(x)[y_1 + y_2 + t_a] \tag{39}$$

Where $M_T(x)$ is the total applied moment.

The bending moment in each adherend, expressed as a function of the total applied moment and the interfacial shear stress, is given as

$$M_1(x) = \frac{R}{R+1}[M_T(x) - b_2\int_0^x \tau(x)(y_1 + y_2 + t_a)dx] \tag{40}$$

$$\text{And, } M_2(x) = \frac{1}{R+1}[M_T(x) - b_2\int_0^x \tau(x)(y_1 + y_2 + t_a)dx] \tag{41}$$

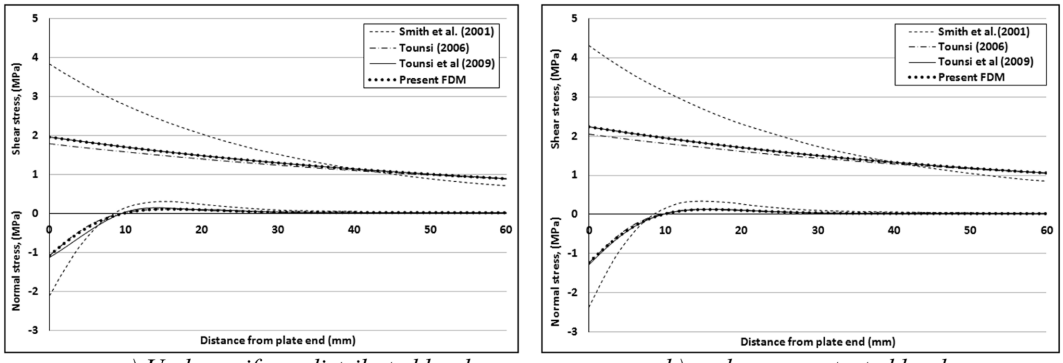

a) Under uniform distributed load *b) under concentrated load*

Fig. 3 Comparaison of interfarcial normal and shear stresses for CFRP-plated rectangular RC beam

The first derivative of the bending moment in each adherend gives

$$\frac{dM_1(x)}{dx} = \frac{R}{R+1}[V_T(x) - b_2\tau(x)(y_1 + y_2 + t_a)] \tag{42}$$

$$\text{And, } \frac{dM_2(x)}{dx} = \frac{1}{R+1}[V_T(x) - b_2\tau(x)(y_1 + y_2 + t_a)] \tag{43}$$

Substituting Eqs. (29) and (30) into Eq. (32) and differentiating the resulting equation yields

$$\begin{aligned}\frac{d^2\tau(x)}{dx^2} = {} & K_S\left(\frac{1}{E_2A_2}\frac{dN_2(x)}{dx} - \frac{y_2}{E_2I_2}\frac{dM_2(x)}{dx} - \frac{y_1}{E_1I_1}\frac{dM_1(x)}{dx} - \frac{1}{E_1A_1}\frac{dN_1(x)}{dx}\right) \\ & -K_S\left[\frac{5t_2}{12G_2} + \frac{1}{t_1G_1A_1}\left(\frac{1}{3}t_0(2t_1 - t_0)\left(\frac{1}{2}t_1 + t_0\right)(b_1 - b_0) + \frac{1}{4}b_0t_1^3\right)\right]\frac{d^2\tau(x)}{dx^2}\end{aligned} \tag{44}$$

Substitution of the shear forces (Eqs. (42) and (43)) and axial forces (Eqs. (35) and (36)) into Eq. (44) gives the following governing differential equation for the interfacial shear stress

$$\frac{d^2\tau(x)}{dx^2} - Kb_2\left(\frac{(y_1 + y_2)(y_1 + y_2 + t_a)}{E_1I_1 + E_2I_2} + \frac{1}{E_1A_1} + \frac{1}{E_2A_2}\right)\tau(x) + K_1\left(\frac{y_1 + y_2}{E_1I_1 + E_2I_2}\right)V_T(x) = 0 \tag{45}$$

$$\text{Where, } K_1 = \frac{1}{\left(\frac{t_a}{G_a} + \frac{t_1}{4G_1}\xi + \frac{5t_2}{12G_2}\right)} \tag{46}$$

And is a geometrical coefficient which is given as

$$\xi = \frac{1}{t_1^2A_1}\left(\frac{4}{3}t_0(2t_1 - t_0)\left(\frac{1}{2}t_1 + t_0\right)(b_1 - b_0) + b_0t_1^3\right) \tag{47}$$

For a rectangular section ($b_1 = b_0$), $\xi = 1$ which corresponds to the same expression given by Tounsi *et al*. (2009) by neglecting shear deformations of the FRP plate. However, for I-beam section we have $\xi < 1$.

4. Normal stress distribution along the FRP-beam interface

The interfacial normal stress in the adhesive can be expressed as follows

$$\sigma_n(x) = K_n \Delta W(x) = K_n[W_2(x) - W_1(x)] \tag{48}$$

Where K_n is the normal stiffness of the adhesive per unit length and can be written as

$$K_n = \frac{\sigma_n(x)}{\Delta W(x)} = \frac{\sigma_n(x)}{\Delta W(x)/t_a}\left(\frac{1}{t_a}\right) = \frac{E_a}{t_a} \tag{49}$$

$W_2(x)$ are $W_1(x)$ the normal displacement of adherends 1 and 2, respectively.
Differentiating Eq.(48) twice results in

$$\frac{d^2\sigma_n(x)}{dx^2} = K_n\left[\frac{d^2W_2(x)}{dx^2} - \frac{d^2W_1(x)}{dx^2}\right] \tag{50}$$

Considering the moment-curvature relationships for the beam and the external reinforcement, respectively, gives

$$\frac{d^2W_1(x)}{dx^2} = \frac{M_1(x)}{E_1I_1} \text{ and } \frac{d^2W_2(x)}{dx^2} = -\frac{M_2(x)}{E_2I_2} \tag{51}$$

The equilibrium of adherends 1 and 2, leads to the following relationships

$$\text{Adherend 1: } \frac{dM_1(x)}{dx} = V_1(x) - b_2y_1\tau(x) \text{ and } \frac{dV_1(x)}{dx} = -b_2\sigma_n(x) - q \tag{52}$$

$$\text{Adherend 2: } \frac{dM_2(x)}{dx} = V_2(x) - b_2y_2\tau(x) \text{ and } \frac{dV_2(x)}{dx} = b_2\sigma_n(x) \tag{53}$$

Based on the above equilibrium equations, the governing differential equations for the deflection of the adherends 1 and 2, expressed in terms of the interfacial shear and normal stresses, are given as follows

$$\text{Adherend 1: } \frac{d^4W_1(x)}{dx^4} = \frac{1}{E_1I_1}b_2\sigma(x) + \frac{y_1}{E_1I_1}b_2\frac{d\tau(x)}{dx} + \frac{q}{E_1I_1} \tag{54}$$

$$\text{Adherend 2: } \frac{d^4W_2(x)}{dx^4} = \frac{-1}{E_2I_2}b_2\sigma(x) + \frac{y_2}{E_2I_2}b_2\frac{d\tau(x)}{dx} \tag{55}$$

Substitution of Eqs. (54) and (55) into the fourth derivation of the interfacial normal stress obtainable from Eq. (48) gives the following governing differential equation for the interfacial normal stress

$$\frac{d^4\sigma_n(x)}{dx^4} + \frac{E_a b_2}{t_a}\left(\frac{1}{E_1 I_1} + \frac{1}{E_2 I_2}\right)\sigma_n(x) + \frac{E_a b_2}{t_a}\left(\frac{y_1}{E_1 I_1} - \frac{y_2}{E_2 I_2}\right)\frac{d\tau(x)}{dx} + \frac{qE_a}{t_a E_1 I_1} = 0 \tag{56}$$

5. Finite difference solution

The governing differential equations for shear stress (Eq. (45)) and normal stress (Eq. (56)) are valid for plated beams with geometric and material properties that are constant along its length. However, in case of complex plate-end geometry (taper) a closed form solution is not possible. A finite difference method can be used to evaluate the adhesive stresses for cases with varying section properties.

A finite difference solution using constant node spacing, h, is outlined below. The nodes are numbered with real nodes from $x = 0$ to $x = L/2$, in addition to virtual nodes (1, 2, $n+3$, $n+4$) which are used to allow derivatives to be defined at nodes 3 and n+2. Subscripts are used to define nodes' numbers in the following equations. In order to obtain accurate results, a fine mesh of 4000 nodes was used.

5.1. Interfacial shear stress

The governing differential equation (Eq. 45) for the interfacial shear stress is simplified as

$$\frac{d^2\tau}{dx^2} + f_1\frac{d\tau}{dx} = f_2 V(x) \tag{57}$$

Where

$$f_1 = -K_1 b_2\left(\frac{(y_1 + y_2)(y_1 + y_2 + t_a)}{E_1 I_1 + E_2 I_2} + \frac{1}{E_1 A_1} + \frac{1}{E_2 A_2}\right) \tag{58}$$

$$f_2 = -K_1\left(\frac{y_1 + y_2}{E_1 I_1 + E_2 I_2}\right) \tag{59}$$

Which can be written in finite difference format as

$$\frac{\tau_{(i-1)} - 2\tau_{(i)} + \tau_{(i+1)}}{h^2} + f_1\tau_{(i)} = f_2 V(x)\ ;\ i = 3\ldots(no+2) \tag{60}$$

Considering the following boundary conditions:

1)- due to symmetry the shear stress at mid-span is zero

$$\tau\left(\frac{L}{2}\right) = \tau_{(n+2)} = 0 \tag{61}$$

2)- at the end of FRP plate, the longitudinal force $N_1(0) = N_2(0) = 0$ and the moment $M_2(0)$ are zero.

As a result, the moment in the section at the plate curtailment is resisted by the beam alone. Thus

$$M_1(0) = M_T(0) = \frac{qa}{2}(L-a) \tag{62}$$

Using this boundary condition in Eq. (32)

$$\frac{d\tau(x=0)}{dx} = -m_2 M_T(0) \tag{63}$$

Where

$$m_2 = \frac{K_1 y_1}{E_1 I_1} \tag{64}$$

Eq. (63) can be written as

$$\frac{-\tau_{(2)} + \tau_{(4)}}{2h} = -m_2 M_T(0) \tag{65}$$

By writing Eq. (60) at the plate-end (node 3) and eliminating τ_2 using Eq. 65, we get

$$(h^2 f_1 - 2)\,\tau_{(3)} + 2\,\tau_{(4)} = h^2 f_2 - 2m_2 h M_T(0) \tag{66}$$

Finally, by combining Eqs. (60), (61), and (66) gives

$$\begin{bmatrix} (f_1 h^2 - 2) & 2 & & & \\ 1 & (f_1 h^2 - 2) & 1 & & \\ & \ddots & \ddots & \ddots & \\ & & 1 & (f_1 h^2 - 2) & 1 \\ & & & & 1 \end{bmatrix} \begin{Bmatrix} \tau_{(3)} \\ \tau_{(4)} \\ \vdots \\ \tau_{(n+1)} \\ \tau_{(n+2)} \end{Bmatrix} = \begin{Bmatrix} h^2 f_2 - 2m_2 h M_T(0) \\ f_2 h^2 V(x) \\ \vdots \\ f_2 h^2 V(x) \\ 0 \end{Bmatrix} \tag{67}$$

These n simultaneous equations are solved explicitly to find the plate force at each of the n nodes

5.2. Interfacial normal stress

A fourth order finite – difference solution is required to find the normal shear stress. The governing equation for normal stress (Eq. (56)) is written at each node ($i = 3 \ldots n + 2$) along the beam

$$\frac{d^4 \sigma_n(x)}{dx^4} + g_1 \sigma_n(x) = g_2 \frac{d\tau(x)}{dx} + g_3 \tag{68}$$

Where

$$g_1 = \frac{E_a b_2}{t_a}\left(\frac{1}{E_1 I_1} + \frac{1}{E_2 I_2}\right) \tag{69}$$

$$g_2 = -\frac{E_a b_2}{t_a}\left(\frac{y_1}{E_1 I_1} - \frac{y_2}{E_2 I_2}\right) \tag{70}$$

$$g_3 = -\frac{qE_a}{t_a E_1 I_1} \tag{71}$$

Eq. (68) can be written in finite difference at i^{th} node as

$$\frac{\sigma_{n(i-2)} - 4\sigma_{n(i-1)} + 6\sigma_{n(i)} - 4\sigma_{n(i+1)} + \sigma_{n(i+2)}}{h^4} + g_1 \sigma_{n(i)} = g_2 \frac{d\tau(x)}{dx} + g_3 \quad i = 3, \ldots n+2 \tag{72}$$

Boundary conditions:

1)- At center the normal stress is zero

$$\sigma_n(x{=}L/2) = \sigma_{n(n+2)} = 0 \tag{73}$$

2)- At the plate ends, the bending moment equals to zero. By Substituting Eq. (51) into Eq. (50) and expressing the result at the plate-end ($x = 0$) yields

$$\left.\frac{d^2\sigma_n(x)}{dx^2}\right|_{x=0} = \frac{E_a}{t_a}\left(\frac{M_1(0)}{E_1 I_1} - \frac{M_2(0)}{E_1 I_1}\right) \tag{74}$$

The boundary condition leads to $M_2(0) = 0$ and $M_1(0) = M_T(0)$, thus the Eq. (74) can be expressed as

$$\left.\frac{d^2\sigma_n(x)}{dx^2}\right|_{x=0} = \frac{E_a}{t_a}\frac{M_T(0)}{E_1 I_1} \tag{75}$$

in finite difference format

$$\frac{\sigma_{n(2)} - 2\sigma_{n(3)} + \sigma_{n(4)}}{h_2} = \frac{E_a}{t_a}\frac{M_T(0)}{E_1 I_1} \tag{76}$$

3)- The shear force at the plate ends equals to zero. Differentiating Eq. 50 and substituting Eq. (52) and (53) into the resulting which may be expressed at the plate-end as follows

$$\left.\frac{d^3\sigma_n(x)}{dx^3}\right|_{x=0} = \frac{E_a}{t_a}\left(\frac{V_1(0)}{E_1 I_1} - \frac{V_2(0)}{E_2 I_2}\right) - \frac{E_a b_2}{t_a}\left(\frac{y_1}{E_1 I_1} - \frac{y_2}{E_2 I_2}\right)\tau(0) \tag{77}$$

The boundary condition leads to $V_2(0) = 0$ and $V_1(0) = V_T(0)$, thus the Eq. (77) can be expressed as

$$\left.\frac{d^3\sigma_n(x)}{dx^3}\right|_{x=0} = \frac{E_a}{t_a}\frac{V_T(0)}{E_1 I_1} + g_2\tau(0) \tag{78}$$

which can be expressed in finite difference format as

$$\frac{-\sigma_{n(1)}+2\sigma_{n(2)}-2\sigma_{n(4)}+\sigma_{n(5)}}{2h^3} = \frac{E_a}{t_a}\frac{V_T(0)}{E_1 I_1}+g_2\tau(0) \tag{79}$$

Eq. (72) can be written at node 3 after eliminating σ_1 and σ_2 using Eqs. (76) and (79) as follows

$$\sigma_{n(3)}(2+h^4 g_1)-4\sigma_{n(4)}+2\sigma_{n(5)} = h^4\left(g_2\frac{d\tau(x)}{dx}+g_3\right)+2h^3\left(\frac{E_a}{t_a}\frac{V_T(0)}{E_1 I_1}+g_2\tau(0)\right)+2h^2\frac{E_a}{t_a}\frac{M_T(0)}{E_1 I_1} \tag{80}$$

Also, at node 4, the Eq. (72) can be written after eliminating σ_2 using Eq. (76) as

$$-2\sigma_{n(3)}+\sigma_{n(4)}(5+h^4 g_1)-4\sigma_{n(5)}+\sigma_{n(6)} = h^4\left(g_2\frac{d\tau(x)}{dx}+g_3\right)-h^2\frac{E_a}{t_a}\frac{M_T(0)}{E_1 I_1} \tag{81}$$

Finally, combining Eqs. (73), (80), and (81) yields a system of n simultaneous equations as follows

$$\begin{bmatrix}
(2+h^4g_1) & -4 & 2 & & & & & & \\
-2 & (5+h^4g_1) & -4 & 1 & & & & & \\
1 & -4 & (6+h^4g_2) & -4 & 1 & & & & \\
 & & & \ddots & & & & & \\
 & & & & 1 & -4 & (6+h^4g_2) & -4 & 1 \\
 & & & & & 1 & -4 & (6+h^4g_2) & -4 \\
 & & & & & & & & 1
\end{bmatrix}
\begin{Bmatrix}
\sigma_{n(3)} \\ \sigma_{n(4)} \\ \sigma_{n(5)} \\ \vdots \\ \sigma_{n(n)} \\ \sigma_{n(n+1)} \\ \sigma_{n(n+2)}
\end{Bmatrix}$$

$$\begin{Bmatrix}
h^4\left(g_2\frac{d\tau(x)}{dx}+g_3\right)+2h^3\left(\frac{E_a}{t_a}\frac{V_T(0)}{E_1 I_1}+g_2 T(0)\right)+2h^2\frac{E_a}{t_a}\frac{M_T(0)}{E_1 I_1} \\
h^4\left(g_2\frac{d\tau(x)}{dx}+g_3\right)-h^2\frac{E_a}{t_a}\frac{M_T(0)}{E_1 I_1} \\
g_2\frac{d\tau(x)}{dx}+g_3 \\
\vdots \\
g_2\frac{d\tau(x)}{dx}+g_3 \\
g_2\frac{d\tau(x)}{dx}+g_3 \\
0
\end{Bmatrix} \tag{82}$$

These n simultaneous equations are solved explicitly for normal stress at each of the n nodes. The normal stress distribution follows

6. Results and discussion

6.1. FRP Plate with constant thickness (without taper)

Two types of beams are used for the present study. The first beam is a rectangular beam with span of 3,000 mm bonded with carbon fiber plastics subjected two cases of loading, uniformly distributed load (UDL) of q = 50kN/m and mid-point load F = 150 kN, the distance between the end of the plate and the support is 300 mm. The geometric and material properties of the beam are given in Table 1. This beam is used mainly to validate the finite difference procedure with the exact solution presented by Tounsi *et al.* (2009). The obtained results are also compared against Smith *et al.* (2001) and Tounsi (2006).

The results obtained from the second I-section steel beam which was carried out by Deng *et al.* (2004) and Belakhdar *et al.* (2010) are used for comparison with present method since the effect of transverse shear has been included in addition to shear correction factor (ξ). The span of the I-section beam is 5,000 m, the distance from the support to the end of the plate is 500mm. the beam is subjected to two cases of loading, uniformly distributed load q = 500 kN/m² and mid-point load F = 500 kN. The cross section properties of I-beam and the material properties are listed in Table 2.

The interfacial shear and normal stresses predicted from the rectangular beam are given in Table 3

Table 1 Dimensions and material properties of the rectangular composite beam

Component	Width b [mm]	Depth t [mm]	Young's modulus E [GPa]	Poisson's ratio	Shear modulus G [Gpa]
Beam	200	300	30,000	0.18	-
Adhesive layer	200	2	3,000	0.35	-
CFRP plate	200	4	140,000	0.28	5,000

Table 2 Dimensions and material properties of the I-section composite beam

Component	Width b [mm]	Depth t [mm]	Young's modulus E [GPa]	Poisson's ratio	Shear modulus G[Gpa]
Beam	b_0 = 211.9 b_1 = 12.7	t_0 = 544.5 t_1 = 21.3	210	0.3	-
Adhesive layer	211.9	2	10	0.3	3.7
FRP plate	211.9	12	310	0.3	3.7

Table 3 comparison of maximum interfacial stresses for the rectangular beam

	Uniform distributed load		Concentrated load	
	Shear stress (MPa)	Normal stress (MPa)	Shear stress (MPa)	Normal stress (MPa)
Smith *et al.* (2001)	3.83	−2.10	4.31	−2.36
Tounsi (2006)	1.79	−1.08	2.05	−1.23
Tounsi *et al.* (2009)	1.96	−1.13	2.24	−1.28
Present FDM	1.96	−1.07	2.24	−1.22

Table 4 comparison of maximum interfacial stresses for the I-section beam

	Uniform distributed load		Concentrated load	
	Shear stress (MPa)	Normal stress (MPa)	Shear stress (MPa)	Normal stress (MPa)
Deng *et al*. (2004)	17.40	13.30	15.00	11.20
Belakhdar *et al*. (2010)	14.00	10.43	14.80	11.05
Present FDM	9.46	7.10	8.23	6.19

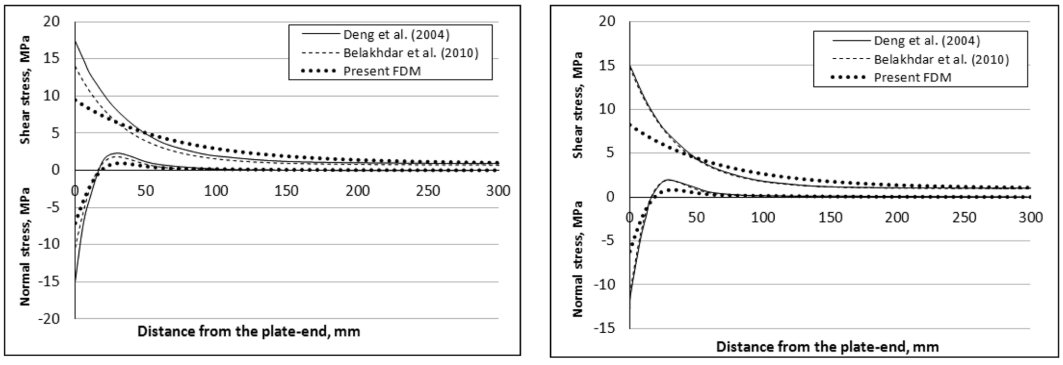

a) Under uniform distributed load *b) under concentrated load*

Fig. 4 Comparaison of interfacial normal and shear stresses for CFRP-plated I-section steel beam

and Fig. 3. The results obtained by Tounsi *et al*. (2009) and the present finite difference method (FDM) are identical which confirm the validity of the FDM.

On the other hand, the results of Tounsi *et al*. (2009) which uses parabolic distribution of shear deformation and results of Tounsi (2006) which uses a linear distribution of shear deformation give lower maximum shear and normal stresses compared with that of Smith *et al*. (2001) which have not included the shear deformation variation effect. Therefore, including shear deformation effect in beam and plate leads to lower value of maximum shear and normal stress.

According to Table 4 and Fig. 4 it is noted that the results obtained from I-section beam also confirm that the inclusion of the shear deformation effect decreases the interfacial maximum stresses noting that the present method takes into account the shear correction factor in case of I-section beam, while Deng *et al*. (2004) method and Belakhdar *et al*. (2010) method have not included neither shear deformation effect nor shear correction factor.

6.2. FRP Plate with taper

Herein the effect of FRP plate with a generally variable thickness is presented. The thickness of the FRP plate $t_2 = t_2(x)$ is described by arbitrary function of the longitudinal coordinate x; hence the cross-sectional area and the second moment of area of the FRP plate, $A_2(\boldsymbol{x})$ and $I_2(x)$, are also functions of the coordinate x. Six particular cases are examined as shown in Fig. 5. Noting that in this parametric study, the I-section steel beam is chosen to be studied where its geometric and materials properties are kept fixed. Thus, only the taper geometric properties are studied according to the following patterns:

Type A: linear variation

$$t_2(x) = \begin{cases} \frac{t_2 - t_e}{a}x + t_e & \text{for} \quad 0 \le x \le a \\ t_2 & \text{for} \quad a \le x \le \frac{L}{2} \end{cases} \tag{83}$$

Type B: Tangent – parabolic variation

$$t_2(x) = \begin{cases} \frac{t_2 - t_e}{a^2}x^2 + t_e & \text{for} \quad 0 \le x \le a \\ t_2 & \text{for} \quad a \le x \le \frac{L}{2} \end{cases} \tag{84}$$

Type C: Parabolic variation

$$t_2(x) = \begin{cases} -\frac{t_2 - t_e}{a^2}x^2 + 2\frac{t_2 - t_e}{a}x + t_e & \text{for} \quad 0 \le x \le a \\ t_2 & \text{for} \quad a \le x \le \frac{L}{2} \end{cases} \tag{85}$$

Type D: stepped tangent – parabolic variation: where the steps gradation follows the same equation defined by Eq. (84). The top layer has a thickness of t_e and the other five layers have the same thickness equals to $(t_2 - t_e) / 5$.

Type E: Stepped parabolic variation: where the steps gradation follows the same equation defined by Eq. (85). The top layer has a thickness of t_e and the other five layers have the same thickness equals to $(t_2 - t_e) / 5$.

The FRP plate with constant thickness (type 0) will be regarded as the reference case. A numerical

Table 5 Maximum interfacial stresses and percent of reduction in maximum stresses for different taper profiles

	Max shear stress τ, [MPa]	$\frac{\tau_{Type(0)} - \tau}{\tau_{type(0)}}$ [%]	Max shear stress σ, [MPa]	$\frac{\sigma_{Type(0)} - \sigma}{\sigma_{type(0)}}$ [%]
Type (0)	9.46	-	−7.10	-
Type (A)	5.34	43.6%	−2.91	59.1%
Type (B)	4.65	50.8%	−2.37	66.7%
Type (C)	5.91	37.5%	−3.42	51.8%
Type (D)	4.68	50.5%	−2.38	66.5%
Type (E)	4.49	52.5%	−2.28	67.9%
Type (F)	5.11	45.9%	−2.62	63.2%

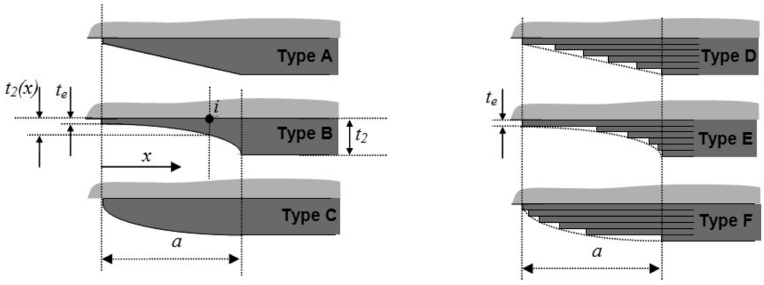

Fig. 5 Taper patterns of FRP plate.

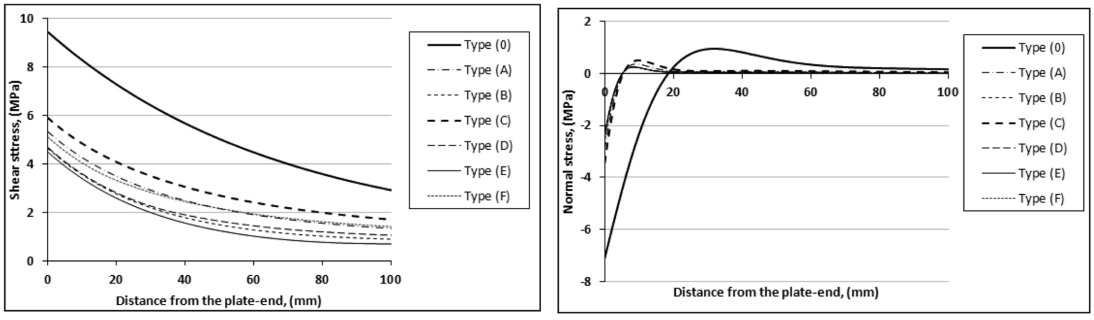

Fig. 6 Interfacial stress for various thickness taper of FRP plate.

study is then conducted to supply information on the contribution of the shape of the thickness profile on the reduction of edge interfacial stresses. In this study, the plated beam is subjected to uniform distributed load of 500 kN/m^2, the length of the taper is a = 200 mm and the thickness at the end of the tape is $t_e = 2\ mm$.

From the results presented in Table 5, we can observe that the decrease of the thickness of the FRP plate in the edge region leads to a reduction in the edge stresses. We can also conclude that FRP plate of type (E) gives an important reduction in edges interfacial stresses, where a reduction of about 52% and 68% in shear and normal stresses, respectively, is obtained. Fig. 6 describes the typical stress field to clarify the comparison of the results with those of the reference case (FRP plate with constant thickness, Type (0)). Hence, reducing the thickness of the FRP plate in the edge region may be considered as an effective way for reducing the magnitude of the edge stresses involved.

6.3. Parametric study

Various parameters influence the maximum values of the shear and normal stresses in the bonding region. In this study we used the taper of all types given in Fig. 5. For retrofitted beams, the most important ones are the thickness and shear modulus of the adhesive, and the thickness and the elastic modulus of the FRP plate. These parameters were studied by several authors (Benyoucef *et al.* 2006, Yang *et al.* 2007, Benyoucef *et al.* 2007). In the present study, we intend to show how the maximum adhesive stresses are influenced by the dimension of the taper. The important parameters of the taper are: the length of the taper (a) and the thickness at the end of the taper (t_e). Figs. 7 and 8 show the maximum interfacial

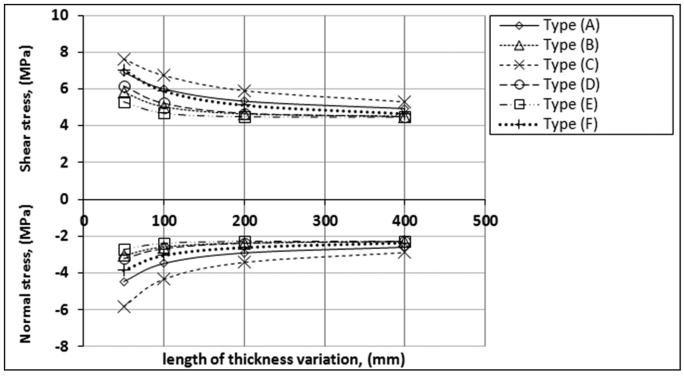

Fig. 7 Maximum interfacial stresses in terms of taper length for different taper profiles.

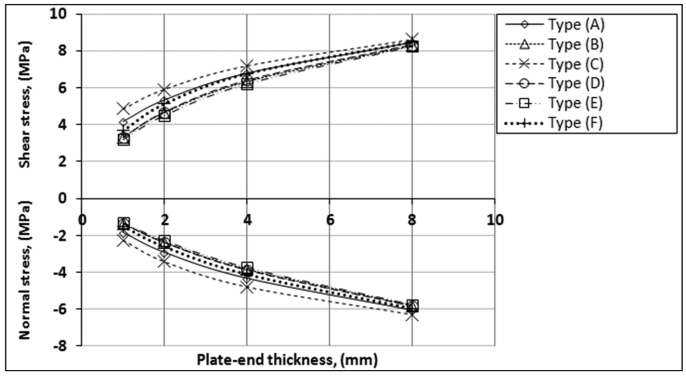

Fig. 8 Maximum interfacial stresses in terms of plate-end thickness for different taper profiles.

stresses at the tapered end of the plate versus the length of the taper and the thickness end, respectively.

Generally, the parametric study indicates the beneficial effect of having a thin tapered end and a long taper. For the latter, the benefit appears to have saturated when the length of the taper is beyond 400 mm.

According to type of taper, it can be noted that the shape of taper has a sensible effect on maximum interfacial stresses. However it seems that the taper shape has a negligible effect on the maximum stresses when length of the taper (a) is grater that 400 mm or the plate-end thickness is greater than 60% of the plate thickness.

7. Conclusions

The present study has developed a relatively simple procedure for evaluating the high shear and normal stress concentrations that occur at the edges of the FRP plate in externally strengthened beams. Finite difference method has been employed to solve problems of beams strengthened with plates have complex geometrical extremities.

High stress concentrations occur at the free ends of adhesively bonded plates. Using the tapered edges, however, reduce the maximum shear stresses by at least 15% the maximum stresses. In addition,

it has been shown that the shape of the taper has an important effect on the reduction of such stresses, where tangent parabolic stepped taper can reduce better the maximum stresses compared to other taper shapes, where a reduction of about 52% and 68% in shear and normal stresses, respectively, is obtained. Hence, the taper is very beneficial for avoiding debonding of the FRP plates from the beams as long as the taper length is less that 400mm and the plate-end thickness is less than 60% of the FRP-plate thickness.

The dimensions of the taper also have an influence on the interfacial edge stresses. The maximum shear and normal stresses decrease as the thickness of the end of the taper decreases and the length of the taper increases. However, there is no further change in stress if the length of the taper is increased beyond 400 mm.

References

Belakhdar, K., Tounsi, A., Benyoucef, S., Adda-Bedia E.A. and El Hassar, S. M. (2010), "On the reduction of the interfacial stresses in a repaired beam with an adhesively bonded FRP plate", *Compos. Interfaces*, **17(**1), 1-14.

Benyoucef, S., Tounsi, A., Meftah, S.A. and Adda-Bedia, E.A. (2006), "Approximate analysis of the interfacial stress concentrations in FRP-RC hybrid beams", *Compos. Interfaces,* **13**(7), 561-571.

Benyoucef, S., Tounsi, A., Meftah, S.A. and Adda-Bedia, E.A.(2007), "Creep and shrinkage effect on adhesive stresses in RC beams strengthened with composite laminates", *Compos. Sci. Technol.,* **67**(6), 933-942.

Deng, J., Marcus, M.K.L. and Stuart, S.J.M. (2004), "Stress analysis of steel beams reinforced with a bonded CFRP plate", *Compos. Struct.*, **65**(2), 205-215.

Gao, B., Kim, J.K. and Leung, C.K.Y. (2006), "Optimization of tapered end design for FRP strips bonded to RC beams", *Compos. Sci. Technol,***66**(10), 1266-1273

Hashemi S. H., Maghsoudi A. A. and Rahgozar R. (2008), "Flexural ductility of reinforced HSC beams strengthened with CFRP sheets", *Struct Eng Mech*, **30**(4).

Lee H. K., Ha S. K. and Afzal M. (2008), "Finite element analysis of shear-deficient RC beams strengthened with CFRP strips/sheets", *Struct. Eng. Mech*, **30**(2), 247-261.

Li, G. and Ghebreyesus, A. (2006), "Fast repair of damaged RC beams using UV curing FRP composites", *Compos. Struct.* **72**(1), 105-110.

Malek, A. M., Saadatmanesh, H. and Ehsani, M. R. (1998), "Prediction of failure load of R/C beams strengthened with FRP plate due to stress concentration at the plate end" *ACI Struct. J.*, **95**(2), 142-152.

Mo, Y.L., Tsai, S.P. and Lee, I.S. (1998), "Seismic performance behaviour of beam – column connections in pre – stressed concrete bridges", *J. Mater. Struct.*, **31**(6), 411-417.

Pesic, N. and Pilakoutas, K., (2005), "Flexural analysis and design of reinforced concrete beams with externally bonded FRP reinforcement", *Mater. Struct.***38**(2), 183-192.

Roberts, T.M. (1989), "Approximate analysis of shear and normal stress concentrations in adhesive layer of plated RC beams", *Struct. Eng.*, **67**(12), 229-233.

Seible, F., Priestley, M.J.N., Hegemier, G.A. and Innamorato, D. (1997), "Seismic retrofit of RC columns with continuous carbon fibre jackets", *J. Comp. Constr.*, **1**(2), 52-62.

Smith, S.T., and Teng, J.G. (2001), "Interfacial stresses in plated RC beams" *Eng. Struct.*, **23**(7), 857-871.

Stratford, T., and Cadei, J. (2006), "Elastic analysis of adhesion stresses for the design of a strengthened plate bonded to a beam" *Constr. Build. Mater.,* **20**(1-2), 34-35.

Tounsi, A. (2006), "Improved theoretical solution for interfacial stresses in concrete beams strengthened with FRP plate", *Int. J. Solids Struct.,* **43**(14-15), 4154-4174.

Tounsi, A. and Benyoucef, S. (2007), "Interfacial Stresses in Externally FRP Plated Concrete Beams", *Int. J. Adhes. Adhes.,* **27**(3), 207-215.

Tounsi, A., Hassaine, T. D., Benyoucef, S. and Adda-Bedia, E.A, (2009), "Interfacial stresses in FRP-plated beams: Effect of adherend shear deformation", *Int. J. Adhes. Adhes.* **29**, 343-351.

Tsai, M.Y., Oplinger, D.W. and Morton, J. (1998), " Improved theoretical solutions for adhesive lap joints", *Int. J. Solids Struct.*, **35**(12), 1163-1185.

Wu H. L. and Wang Y. F. (2010), "Experimental study on reinforced high-strength concrete short columns confined with AFRP sheets", *Steel Compos Struct*, **10**(6).

Yang, J., Ye, J. and Niu, Z. (2007), "Interfacial shear stress in FRP-plated RC beams under symmetric loads", *Cem. Concr. Compos.*, **29**(5), 421-432.

Yuan, H. and Lin, Z. (2009), **"**Theoretical model on interface failure mechanism of reinforced concrete continuous beam strengthened by FRP", *Acta Mechanica Solida Sinica,* **22**(2), 161-170**.**

Zhu Y. and Zhang Y. X. (2010), "Nonlinear finite element analyses of FRP-reinforced concrete slabs using a new layered composite plate element", *Comput. Mech.* **46**(3), 410-430.

CC